crystals

MDPI

Article

Isocyanide π-Hole Interactions Supported by Aurophilic Forces

Andrey S. Smirnov [1], Mikhail A. Kinzhalov [1], Rosa M. Gomila [2], Antonio Frontera [2], Nadezhda A. Bokach [1] and Vadim Yu. Kukushkin [1,3,*]

[1] Institute of Chemistry, St. Petersburg State University, Universitetskaya Nab. 7/9, Saint Petersburg 199034, Russia
[2] Department of Chemistry, Universitat de les Illes Balears, Crta. de Valldemossa km 7.5, 07122 Palma de Mallorca, Spain; r.gomila@uib.es
[3] Laboratory of Crystal Engineering of Functional Materials, South Ural State University, 76, Lenin Av., Chelyabinsk 454080, Russia
* Correspondence: v.kukushkin@spbu.ru

Abstract: Treatment of the [AuCl(tetrahydrothiophene)] complex with 4-chloro-2-iodo-1-isocyanobenzene furnished the gold(I) compound [AuCl(CNC_6H_3-4-Cl-2-I)] (**1**). In the crystal structure of **1**, the linear C–Au–Cl group is subject to the solid-state head-to-tail pairing, which is determined by the aurophilic Au···Au and the rare π-hole$_{CN}$···Cl interactions. These two types of structure-determining interactions are complementary to each other, and the system of Au···Au and C_{CN}···Cl contacts accomplishes a 2D extended ladder-type architecture. In addition, the terminal I-atoms are involved in the three-center halogen bonding. Density functional theory calculations, employing a set of computational tools, verified the role of Au···Au and π-hole$_{CN}$···Cl noncovalent bonds in the spectrum of noncovalent forces.

Keywords: gold(I) complexes; isocyanide ligands; π-hole interactions; aurophilic interactions

check for updates

Citation: Smirnov, A.S.; Kinzhalov, M.A.; Gomila, R.M.; Frontera, A.; Bokach, N.A.; Kukushkin, V.Y. Isocyanide π-Hole Interactions Supported by Aurophilic Forces. *Crystals* **2023**, *13*, 1177. https://doi.org/10.3390/cryst13081177

Academic Editor: Vladimir P. Fedin

Received: 10 July 2023
Revised: 24 July 2023
Accepted: 25 July 2023
Published: 28 July 2023

Copyright: © 2023 by the authors. Licensee MDPI, Basel, Switzerland. This article is an open access article distributed under the terms and conditions of the Creative Commons Attribution (CC BY) license (https://creativecommons.org/licenses/by/4.0/).

1. Introduction

Noncovalent interactions (for general reviews, see refs [1–6]) play key roles in various fields of modern science, spanning from chemistry to molecular biology. Despite their low energy, in many instances, they function collectively, and the sum of their actions can significantly affect synthesis [7,8], catalytic transformations (including noncovalent organic catalysis [9,10]), and reactivity of chemical compounds [2]. Currently, a classification of these interactions includes their division into the σ- and π-hole interactions (for reviews on σ- and π-hole interactions, see refs [11–17])—depending on the location of the regions with positive molecular electrostatic potential (abbreviated as MEP). If a σ-hole interaction is associated with the positive MEP on the extension of the covalent σ-bond, a π-hole interaction usually occurs in the direction perpendicular to the σ-framework of the molecular moiety [17].

In the overwhelming majority of cases, most popular π-hole donors, utilized as coformers of noncovalent interaction, include electron-deficient aromatics, while π-hole donor properties of triple-bonded small molecules were revealed in only a few cases, namely, for carbon monoxide [18,19], organic nitriles [20], and cyanamides [21]. Furthermore, it has been previously reported that coordinated isocyanides are chameleonic species [22,23], and they feature either nucleophilic (low-oxidation state metal ions) [24] or electrophilic (high-oxidation state metal ions) characters depending on the identity of a metal site, in particular on their donor/acceptor abilities. When the ligated isocyanides are bound to high-oxidation state metal ions, they could be involved in π-hole···d_z^2-[M], [25] π-hole···π [26], and π-hole···lone pair (LP) [27] interactions.

We report herein on π-hole$_{CN}$···Cl interactions between an isocyano group and a chlorido ligand from the neighboring complex. These contacts have no covalent analogs. The observed type of π-hole$_{CN}$ interaction is supported by and complementary to aurophilic

forces (for reviews on aurophilicity, see refs [28–32]) that occurred in the same compound during its association in the solid state. DFT calculations are used to closely interrogate the bonding in the RNC–Au–Cl linear units that, in the solid state, are assembled in head-to-tail (or, in other words, antiparallel) binding mode. The aurophilic Au···Au and π-hole···LP interactions were characterized using several computational tools.

2. Materials and Methods

2.1. Reagents, Instrumentation, and Methods

Solvents, tetrahydrothiophene (THT), and $HAuCl_4$ were obtained from commercial sources and used as received. 4-Chloro-2-iodo-1-isocyanobenzene [33] and [AuCl(THT)] [34] were prepared according to the published procedures.

The high-resolution mass spectra were obtained on a Bruker micrOTOF spectrometer equipped with an electrospray ionization (ESI) source, and MeOH was used as the solvent. The instrument was operated in positive ion mode with an *m/z* range of 50–3000. The most intensive peak in the isotopic pattern is reported. Infrared spectra (4000–400 cm^{-1}) were recorded on a Shimadzu IRAffinity-1 FTIR spectrophotometer in KBr pellets. NMR spectra were measured on Bruker AVANCE III 400 spectrometers in $CDCl_3$ at ambient temperature (at 400 and 100 MHz for ^1H and ^{13}C NMR, respectively). Chemical shifts are given in δ-values [ppm] referenced to the residual signals of undeuterated solvent ($CHCl_3$): δ 7.27 (^1H) and 77.0 (^{13}C).

Synthesis of **1**: 4-chloro-2-iodo-1-isocyanobenzene (42 mg, 0.16 mmol) was added to a solution of [AuCl(THT)] (50 mg, 0.16 mmol) in CH_2Cl_2 (5 mL), whereupon the reaction mixture was stirred for 40 min at 20 °C. The resulting suspension was evaporated at room temperature under reduced pressure (20 mbar) to dryness. The colorless residue was washed with Et_2O (two 2-mL portions) and then dried in the air at room temperature. Yield is 77 mg or 98%. Colorless solid. Calcd (%) for $C_7H_3NAuCl_2I$: C 16.96, H 0.61, N 2.82; Found: C 17.11, H 0.70, N 2.73. ESI $HRMS^+$ (MeOH, *m/z*): 517.8251 ([**1** + Na]$^+$, calcd. for $C_7H_3NAuCl_2INa^+$ 517.8250). FTIR, ν_{max} (KBr, cm^{-1}): 2221 ν(C≡N). ^1H NMR ($CDCl_3$, δ): 7.47–7.51 (m, 1H), 7.51–7.55 (m, 1H), 7.97 (d, 1H, $^3J_{H,H}$ = 2 Hz). $^{13}C\{^1H\}$ [7] NMR ($CDCl_3$, δ): 95.3, 128.0, 128.7, 130.0, 138.3, 139.9, 144.6.

2.2. X-ray Diffraction Study

Crystals of **1** were obtained by slow evaporation of its CH_2Cl_2 solution at room temperature. Single-crystal X-ray diffraction experiment was carried out on a SuperNova, single source at offset/far, HyPix3000 diffractometer (Agilent Technologies (Oxford Diffraction), Santa Clara, CA 95051, United States) with monochromated CuKα radiation. Crystal was kept at 100(2) K during data collection. Structures were solved by ShelXT [35] (structure solution program using Intrinsic Phasing) and refined using the ShelXL [36] program incorporated in the OLEX2 program package [37]. Empirical absorption correction was accounted for using spherical harmonics implemented in the SCALE3 ABSPACK scaling algorithm (CrysAlisPro, 1.171.40.71a, Rigaku Oxford Diffraction 2020). Crystallographic details are summarized in Table S1. CCDC number 2280014 contains the supplementary crystallographic data for this paper. These data can be obtained free of charge from the Cambridge Crystallographic Data Centre via www.ccdc.cam.ac.uk/data_request/cif (accessed on 10 July 2023).

2.3. Computational Details

Turbomole 7.7 program and X-ray coordinates were used for the calculations reported herein [38]. The crystallographic coordinates were used because we are interested in evaluating the interactions as they stand in the solid state. The level of theory used for the calculations was PBE0-D3/def2-TZVP [39–41]. For iodine, effective core potentials (ECP) and relativistic effects were used for the inner electrons [42]. The 0.001 a.u. isovalue was used for the MEP surface plots. The quantum theory of atoms in molecules (QTAIM) and noncovalent interaction plot index (NCIplot) methods proposed by Bader [43] and

W. Yang et al. [44] were used to analyze the topology of the electron density and were plotted using the VMD software 1.9.3 [45]. NCIplot index settings: RDG = 0.5 a.u.; cut-off ρ = 0.04 a.u.; and color scale $-0.03 \leq \text{sign}(\lambda_2)\rho \leq 0.03$ a.u. The electron localization function (ELF) [46] analysis was performed using the MultiWFN program [47] at the PBE0-D3/def2-TZVP level of theory.

3. Results and Discussion

3.1. X-ray Diffraction Study

The molecular structure of the gold(I) complex [AuCl(CNC$_6$H$_3$-4-Cl-2-I)] (**1**) (Figure 1) is analogous to those reported for other [AuCl(CNR)] complexes [48–51]. The gold(I) ion is in a linear coordination environment, which is formed by one isocyanide and one chlorido ligand. Bond distances and angles are typical for this type of complex [48–50].

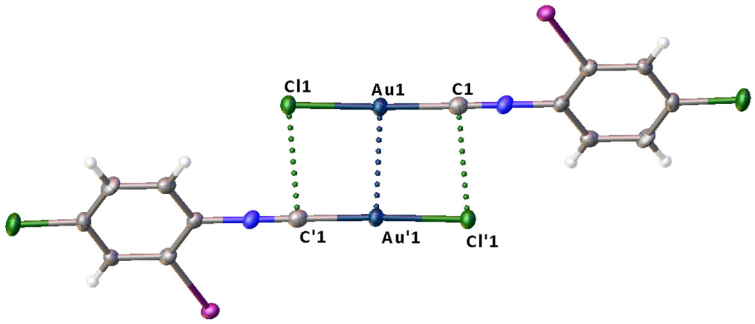


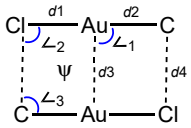
Figure 1. Identified Au···Au and C_{CN}···Cl contacts in the crystal structure of **1**. Symmetry operation used to generate corresponding atoms:' is 1–*x*; 2–*y*; 1–*z*.

In the structure of **1**, each gold(I) center forms several intermolecular contacts. The shortest separation, which involves a metal atom, is Au···Au (3.3050(8) Å; vs. Bondi [52,53] Σ_{vdW} 3.32 Å); this metallophilic bond is characteristic for (RNC)[Au^{I}] species [18,48,50]. The Au···Au contact is involved in the system of noncovalent interactions, which also includes two antiparallel C_{CN}···Cl short separations (3.428(6) Å; vs. Bondi [52,53] Σ_{vdW} 3.50 Å) (Figure 1). The linear C–Au–Cl group is subject to solid-state head-to-tail pairing according to the association mode predicted and studied computationally [18] for similar gold(I) species. Another Au···Au contact in the system of noncovalent interactions includes two C_{CN}···Au and one Au···Au contact. In the latter aurophilic contact, the Au···Au distance is 3.5672(7) Å (Figure S1). It is still larger than the sum of the corresponding Bondi Σ_{vdW}Au + Au = 3.32 Å, but lower than Alvarez [52,53] Σ_{vdW}Au + Au = 4.64 Å.

Other unconventional contacts in the crystal structure are C_{CN}···Cl (3.428(6) Å) and C_{CN}···Au (3.495(5) Å). For the C_{CN}···Cl separation, the C···Cl distance is smaller than Bondi Σ_{vdW}C + Cl 3.45 Å. Geometry considerations based on the data collected in Table 1 indicate that the Cl nucleophilic site is directed to the isocyano carbon. The availability of the π-hole$_{CN}$···LP$_{Cl}$ interaction was confirmed in the appropriate theoretical study (see later).

To find our similarities with the crystal structure of our gold complex, which is based on one Au···Au and two C_{CN}···Cl contacts, we performed a Cambridge Structural Database (CSD). The search criteria included the following parameters: the structures of [AuX(CNR)] (X = Cl, Br, I) exhibiting one Au···Au contact with *d*(Au + Au) < Bondi Σ_{vdW}(Au + Au) and two antiparallel C_{CN}···X with *d*(C + X) < Bondi Σ_{vdW}(C + X). By applying these criteria, we retrieved six structures of [AuCl(CNAr)] species, but only four out of six structures were of acceptable quality (R_w < 5%). Examination of the geometrical parameters of the four structures (Table 1) allows the assignment of these contacts to aurophilic Au···Au and π-hole$_{CN}$···LP$_{Cl}$ interactions.

Table 1. Geometrical parameters of short contacts in [AuCl(CNAr)] structures.



φ is a torsion angle ClAuAuC

CSD Code	*d*1	*d*2	*d*3	*d*4	∠1	∠2	∠3	φ
EBEZAP	2.258(4)	1.929(10)	3.3159(8)	3.373(11)	94.0(3)	86.7(2)	91.6(4)	0.1(3)
EQOGOJ	2.2518(11) 2.2577(11) 2.2530(13) 2.2593(14)	1.923(5) 1.919(4) 1.918(5) 1.935(5)	3.2814(6) 3.2903(7)	3.414(5) 3.436(5) 3.429(5) 3.448(4)	87.34(13) 87.77(13) 87.63(13) 87.37(12)	79.13(8) 79.27(8) 78.94(9) 79.29(9)	97.32(16) 97.71(15) 97.36(15) 97.45(16)	7.57(15) 8.88(14) 8.37(13) 9.57(14)
QIZTEA	2.2564(15) 2.2584(14)	1.946(6) 1.942(6)	3.3092(6)	3.433(6)	90.64(16) 89.91(16)	81.92(10) 82.57(10)	95.24(19) 94.5(2)	3.20(17) 2.88(17)
KEJRUQ	2.255(2) 2.258(2)	1.957(9) 1.939(9)	3.3275(7) 3.2601(7)	3.386(8) 3.410(8)	101.5(2) 92.0(2)	93.51(16) 82.92(18)	83.8(2) 93.4(3)	1.53(19) 1.12(18)
1	2.2639(11)	1.926(6)	3.3050(8)	3.428(6)	92.53(16)	83.77(10)	93.15(19)	0.90(17)

Another unconventional contact is $C_{CN}\cdots$Au, in which the distances between the C-atom of the isocyanide group and the gold(I) site are slightly larger than Bondi Σ_{vdW}C + Au 3.36 Å, but significantly less than Alvarez Σ_{vdW}C + Au = 4.09 Å [54]. The $C_{CN}\cdots$Au contact exhibits a comparable length with those in the earlier reported structures of [AuCl(CNR)] (R = C_6H_4OMe-4; BUVCAX [55]; 3.662(5) Å and R = 2-naphthyl; TAHVIK [56]; 3.605(8) Å) and even in other (RNC)Au^I species (see CSD search with brief analysis for $C_{CN}\cdots$M contacts in refs [25,57]). In these reports, π-hole$\cdots$[Au^I] nature of the C$\cdots$Au contact has not been analyzed, while analogous π-hole$\cdots$[M^{II}] (M = Pd, Pt) contacts were thoroughly investigated, including DFT studies of their nature [25,57].

Based on the angular parameter analysis (both ∠N≡C$\cdots$Au and ∠C$\cdots$Au–C angles are ca. 100°), one can conclude that the C and Au atoms are in contact but parallel displaced. Our theoretical calculations revealed no bond critical point or bond path and only a small value of energetic stabilization due to electron transfer from Au($5d_{x^2-y^2}$) to the π*(C≡N) orbital. As further explained below, the NCIplot analysis also suggests the presence of a weak interaction and confirms that both the CN group and Au atoms are in contact. The existence of such π-$hole_{CN}\cdots$[Au^I] interaction seems quite logical, as the gold(I) site, despite its positive charge, exhibits *d*-orbital nucleophilicity and can function as a nucleophilic coformer of noncovalent interactions, for instance, halogen bonding [58–60]. However, the results of our geometry considerations and the computation data give only a hint that such interaction likely exists, and it is very weak.

The system of Au$\cdots$Au and $C_{CN}\cdots$Cl contacts accomplishes a 2D extended ladder-type architecture (Figure 2) that passes along the *b*-axis. Molecules from different 2D-ladder arrays are linked to each other via I$\cdots$I contacts (3.7932(7) Å vs. Bondi Σ_{vdW}I + I = 3.96 Å) (Figure 3 and Figure S2). These contacts, as follows from consideration of the ∠C–I–I values (150.10(15) and 128.76(14)°), are close to Type-II halogen$\cdots$halogen interactions (idealized angles $\theta_1 \approx 180$ and $\theta_2 \approx 90°$) [61,62]. In addition, molecules from the same 2D-ladder array exhibit short I$\cdots$I contacts (4.0486(1) Å vs. Bondi Σ_{vdW}I + I = 3.96 Å) of Type-I (∠C–I–I values are 103.04(14) and 76.96(14)° that are close to 90°) halogen$\cdots$halogen interactions [62]. To be conclusive regarding the nature of such contacts, an elaborated theoretical study is detailed below, where different computational tools were used to investigate the donor/acceptor role of the I-atoms.

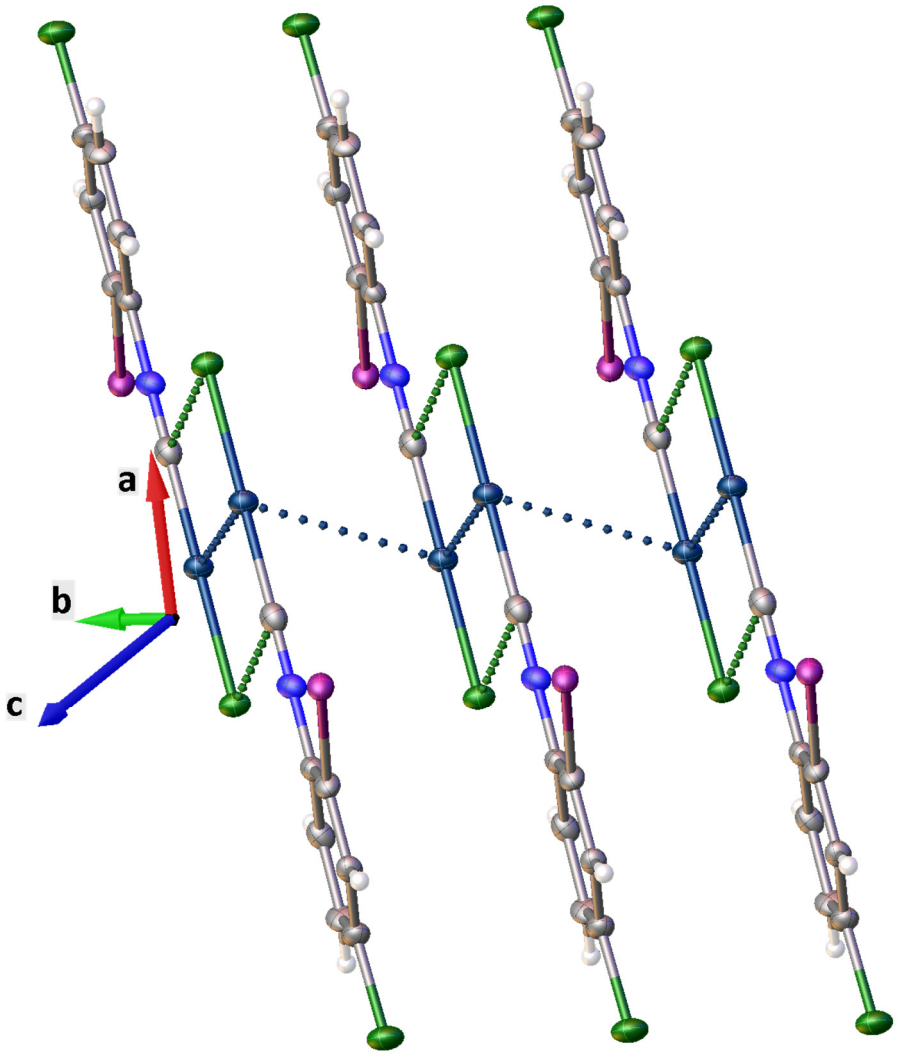


Figure 2. 2D-ladder type architecture occurred via different types of noncovalent interactions. Cell axes (a, b, c) are given for the sake of clarity.

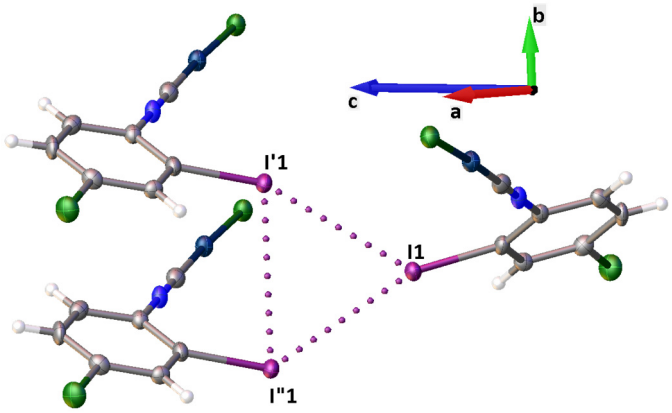


Figure 3. I···I contacts in the crystal structure of **1**. Symmetry operations are used to generate corresponding atoms: 'is $1-x; \frac{1}{2}+y; 3/2-z$ and " is $1-x; -\frac{1}{2}+y; 3/2-z$.

3.2. Theoretical Study

First, the MEP surface was computed to study the electron-rich and electron-poor parts of compound **1**, and the corresponding surface is represented in Figure 4. It can be observed

that the MEP minimum, as expected, is located at the chlorido ligand (−33.8 kcal/mol). The MEP is also negative at the Au and has negative belts around the iodine and chlorine substituents (−5.0 kcal/mol). The MEP maximum is located at the iodine's σ-hole (33.9 kcal/mol), and it is also large and positive at the aromatic H-atoms, ranging from 30 to 34 kcal/mol. The MEP is also positive over the center of the aromatic ring (16.9 kcal/mol), σ-hole of chlorine (18.8 kcal/mol), and over the isocyano group (11.9 over C and 18.5 over N, measured perpendicular to the molecular plane). This electron density distribution explains the formation of the 2D-ladder type architecture with the antiparallel arrangement of the molecules.

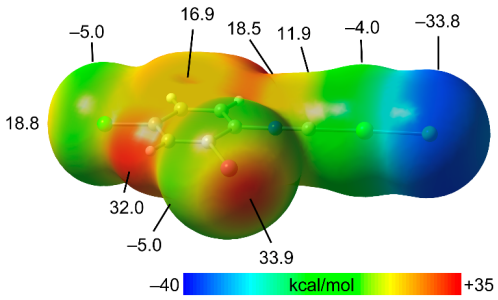


Figure 4. MEP surface of **1**. Energies at selected points are indicated in kcal/mol. Isovalue 0.001 a.u.

To characterize the 2D-ladder packing and gain insight into the nature of the non-covalent interactions, DFT calculations were performed using two independent dimers, denoted as "A" and "B," that exemplify the two binding modes observed in the infinite assembly depicted in Figure 2. The energetic features of the dimers and the QTAIM/NCIplot analyses are given in Figure 5. As can be inferred from consideration of our computational results, both binding modes exhibit very similar interaction energies (−13.6 kcal/mol and −13.4 kcal/mol for dimers A and B, respectively). Both dimers, A and B, are interconnected by five bond critical points (CPs, represented as small red spheres) and bond paths (orange lines). One bond CP interconnects both Au atoms, disclosing the existence of aurophilic interactions. Moreover, in both dimers, the Cl is connected to the isocyano group by a bond CP and bond path, in the case of Dimer A to the C-atom and in the case of Dimer B to the N-atom. Finally, in Dimer A, two symmetrically equivalent CPs and bond paths connect two aromatic CH bonds to the chlorido ligands. For Dimer B, the additional bond CPs and bond paths connect the Cl to one C-atom of the aromatic ring, thus evidencing the occurrence of $\pi\cdots$LP interactions.

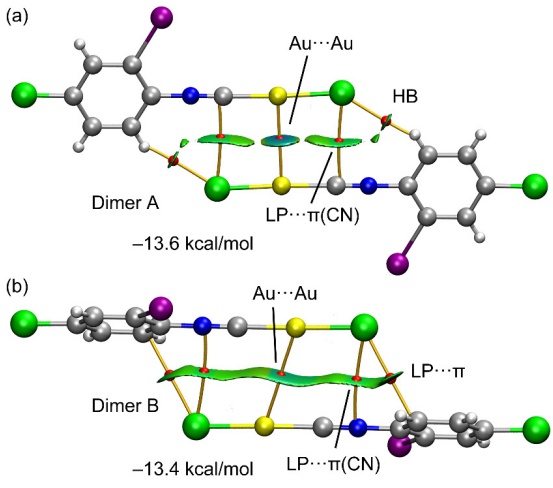


Figure 5. QTAIM and NCIplot analyses of Dimer A (**a**) and Dimer B (**b**). The dimerization energies are indicated. See Section 2.3 for the settings. Only intermolecular interactions are represented.

Such a combination of interactions explains the rather strong dimerization energies. The main difference between both dimers is observed in the NCIplot analysis and the shape of the reduced density gradient (RDG) isosurfaces. Dimer A exhibits well-defined disk-shaped isosurfaces for each contact, revealing that the Au···Au interaction is the strongest (blue RDG isosurface). In contrast, Dimer B presents a continuous and green RDG isosurface, thus suggesting a more complicated (cooperative) binding and supporting the possibility of a partial contribution of π-hole$_{CN}$···[Au^{I}] interaction in combination with the aurophilic one and also π-hole$_{CN}$···Cl contacts.

To shed light on the physical nature interactions in both dimers, we performed the natural bond orbital (NBO) analysis since it is useful to study charge-transfer effects from an orbital donor–acceptor viewpoint. The most important contributions (>1 kcal/mol) obtained from the NBO analysis of both dimers are provided in Figure 6. For Dimer A, two orbital donor–acceptor contributions were found: one corresponds to the aurophilic interaction that is composed by an electron donation from the LP located at the filled $5d_{x^2-y^2}$ atomic orbital of gold to the antibonding C–Au orbital of the adjacent molecule, and vice versa. The associated stabilization energy is $E^{(2)}$ = 3.7 kcal/mol due to $5d_{x^2-y^2}$ [Au]→σ*(C–Au), which is the largest donor–acceptor orbital contribution. In addition, an electron donation from one LP of the chlorido ligand to one of the π*(C≡N) orbitals of the isocyano group is also observed, with a concomitant second-order stabilization of $E^{(2)}$ = 1.4 kcal/mol.

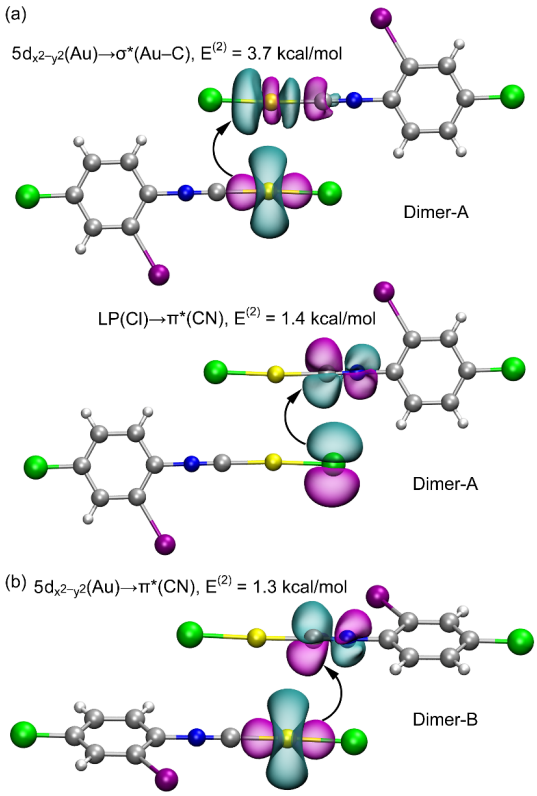


Figure 6. NBOs are involved in the charge transfer in dimers A (**a**) and B (**b**). The second-order perturbation energies are also indicated.

For Dimer B, it is interesting to highlight that the most important charge transfer is from the LP of gold ($5d_{x^2-y^2}$) to the π*(C≡N) orbital, confirming the existence of the interaction between the π-hole at the isocyano group and gold.

Echeverria [18] has also analyzed C$_{CN}$···Cl contacts in Au^{I} dimers similar to those observed in Dimer A (characterized by bond CPs and disk-shaped RDG isosurfaces). The reported NBO stabilization energies ranged from 0.05 to 0.2 kcal/mol for the LP(Cl)→π*(C≡N)

donor–acceptor interactions. This reveals that the $C_{CN}\cdots Cl$ contacts studied herein are stronger than those previously studied.

Finally, the noncovalent three-center I···I contacts in the structure of **1** (Figure 3) were also studied using QTAIM analysis and the electron localization function (ELF) method to verify the halogen bonding (for reviews on halogen bonding, see refs [1–5,63]) nature of these contacts. The results are shown in Figure 7, and it can be observed that the QTAIM analysis reveals the existence of three I···I contacts characterized by the corresponding bond CPs and bond paths. The trimerization energy is moderately strong (−10.3 kcal/mol), likely due to the contribution of the π-stacking of two out of the three molecules that form the I···I triangle. The ELF 2D map is represented in Figure 7b, using the plane defined by the three I-atoms for the orientation. This ELF analysis reveals that the I···I contacts characterized by the bond CPs denoted as "a" and "b" can be defined as halogen bonds since the bond path that connects the I-atoms crosses the LP of one I (electron donor) and the σ-hole of the other one (electron acceptor). In contrast, the bond CP denoted as "c" corresponds to an I···I interaction that cannot be classified as a halogen bond since the bond path crosses the LPs of both iodine atoms pointing to each other. These electron-rich regions are significantly smaller than similar regions (LPs) that are not pointing to each other. This indicates some polarization and/or conjugation of the LPs to the aromatic ring, likely reducing the electrostatic repulsion. This I···I van der Waals contact can be rationalized considering that other forces like dispersion or polarization compensate the electrostatics or that is a consequence of packing effects.

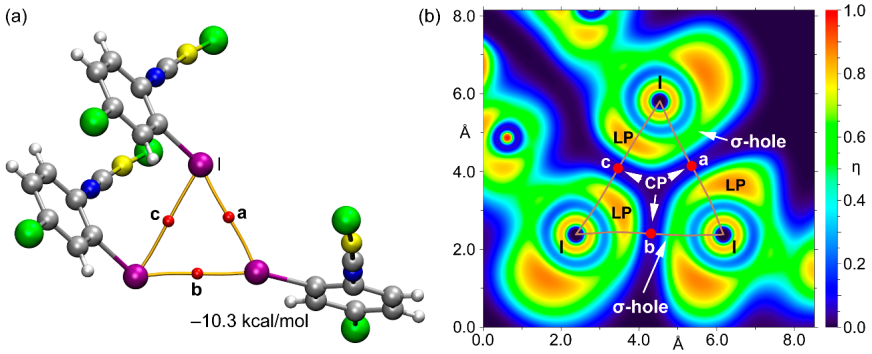


Figure 7. (**a**) QTAIM of the trimeric assembly of compound **1**. (**b**) ELF 2D of the trimer.

4. Conclusions

By inspecting the X-ray structure of gold(I)-based complex **1**, we recognized rare structure-determining $\pi\text{-hole}_{CN}\cdots Cl$ contact that involves an isocyanide ligand acting as a π-hole donor. The observed type of $\pi\text{-hole}_{CN}\cdots LP_{Cl}$ interaction is complementary to the Au···Au aurophilic forces that occurred in the same compound on its head-to-tail association in the solid state. The interplay of these two types of interactions largely determines the crystal structure.

Results of DFT calculations revealed that both binding modes (antiparallel dimers) are energetically similar and that the Au···Au interaction in Dimer A is the most favorable, as shown by the NCIplot and NBO analyses. In the case of Dimer B, the NBO analysis gives a hint for the existence of the rare π-hole···*d*-metal, namely $\pi\text{-hole}_{CN}\cdots[Au^I]$, interaction since LP(Au)→π*(C≡N) charge transfer is observed. Moreover, the RDG isosurface in Dimer B, which embraces the whole region between the NC–Au–Cl, is also compatible with the contribution of the $\pi\text{-hole}\cdots[Au^I]$ interaction. We hope these results will stimulate further studies focused on $\pi\text{-hole}_{CN}\cdots[Au^I]$ systems and eventually lead to discovering a system in which these contacts are unambiguously recognized.

Supplementary Materials: The following supporting information can be downloaded at: https://www.mdpi.com/article/10.3390/cryst13081177/s1, Figure S1: Identified Au···Au and $C_{CN}\cdots Cl$

contacts in the crystal structure of **1**; Figure S2: A view of a fragment of the crystal packing (along the *a* axis) demonstrating 2D-ladder type architecture and I···I HaBs; Table S1: Crystal data and structure refinement for **1**.

Author Contributions: Conceptualization, V.Y.K. and N.A.B.; methodology, A.S.S., M.A.K., R.M.G. and A.F.; investigation, A.S.S., M.A.K. and R.M.G.; writing—original draft preparation, N.A.B., A.F. and A.S.S.; writing—review and editing, V.Y.K.; visualization, N.A.B. and R.M.G.; funding acquisition, A.S.S. All authors have read and agreed to the published version of the manuscript.

Funding: This study was funded by the Russian Science Foundation, project number 22-23-00307.

Data Availability Statement: The data that support the findings of this study are available upon reasonable request from the authors.

Acknowledgments: The article is in commemoration of the 300th anniversary of St. Petersburg State University's founding. Physicochemical studies were performed at the Center for Magnetic Resonance, the Center for X-ray Diffraction Studies, the Center for Thermogravimetric and Calorimetric Research, and the Center for Chemical Analysis and Materials Research (all belonging to Saint Petersburg State University). A. F. is grateful to the Alexander von Humboldt Foundation for the J. C. Mutis Award.

Conflicts of Interest: The authors declare no conflict of interest.

References

1. Shukla, R.; Chopra, D. Chalcogen and pnictogen bonds: Insights and relevance. *Curr. Sci.* **2021**, *120*, 1848–1853. [CrossRef]
2. Cornaton, Y.; Djukic, J.-P. Noncovalent Interactions in Organometallic Chemistry: From Cohesion to Reactivity, a New Chapter. *Acc. Chem. Res.* **2021**, *54*, 3828–3840. [CrossRef]
3. Alkorta, I.; Elguero, J.; Frontera, A. Not Only Hydrogen Bonds: Other Noncovalent Interactions. *Crystals* **2020**, *10*, 180. [CrossRef]
4. Frontera, A.; Bauzá, A. On the Importance of σ–Hole Interactions in Crystal Structures. *Crystals* **2021**, *11*, 1205. [CrossRef]
5. Miller, D.K.; Chernyshov, I.Y.; Torubaev, Y.V.; Rosokha, S.V. From weak to strong interactions: Structural and electron topology analysis of the continuum from the supramolecular chalcogen bonding to covalent bonds. *Phys. Chem. Chem. Phys.* **2022**, 8251–8259. [CrossRef] [PubMed]
6. Schneider, H.-J. Noncovalent interactions: A brief account of a long history. *J. Phys. Org. Chem.* **2022**, *35*, e4340. [CrossRef]
7. *Non-covalent Interactions in the Synthesis and Design of New Compounds*; Maharramov, A.M.; Mahmudov, K.T.; Kopylovich, M.N.; Pombeiro, A.J.L. (Eds.) Wiley Online Library: Hoboken, NJ, USA, 2016.
8. Loh, C.C.J. Exploiting non-covalent interactions in selective carbohydrate synthesis. *Nat. Rev. Chem.* **2021**, *5*, 792–815. [CrossRef]
9. Mahmudov, K.T.; Gurbanov, A.V.; Guseinov, F.I.; Guedes da Silva, M.F.C. Noncovalent interactions in metal complex catalysis. *Coord. Chem. Rev.* **2019**, *387*, 32–46. [CrossRef]
10. Mahmudov, K.T.; Kopylovich, M.N.; da Silva, M.F.C.G.; Pombeiro, A.J. *Noncovalent Interactions in Catalysis*; Royal Society of Chemistry: London, UK, 2019.
11. Bauza, A.; Mooibroek, T.J.; Frontera, A. The Bright Future of Unconventional σ/π-Hole Interactions. *ChemPhysChem* **2015**, *16*, 2496–2517. [CrossRef]
12. Politzer, P.; Murray, J.S. Electrostatics and Polarization in σ- and π-Hole Noncovalent Interactions: An Overview. *ChemPhysChem* **2020**, *21*, 579–588. [CrossRef]
13. Politzer, P.; Murray, J.S.; Clark, T. Halogen bonding and other σ-hole interactions: A perspective. *Phys. Chem. Chem. Phys.* **2013**, *15*, 11178–11189. [CrossRef] [PubMed]
14. Politzer, P.; Murray, J.S.; Clark, T.; Resnati, G. The σ-hole revisited. *Phys. Chem. Chem. Phys.* **2017**, *19*, 32166–32178. [CrossRef] [PubMed]
15. Seth, S.K.; Bauza, A.; Frontera, A. Quantitative analysis of weak non-covalent σ-hole and π-hole interactions. *Monogr. Supramol. Chem.* **2019**, *26*, 285–333.
16. Zierkiewicz, W.; Michalczyk, M.; Scheiner, S. Noncovalent bonds through sigma and Pi-hole located on the same molecule. guiding principles and comparisons. *Molecules* **2021**, *26*, 1740. [CrossRef] [PubMed]
17. Wang, H.; Wang, W.; Jin, W.J. σ-Hole Bond vs π-Hole Bond: A Comparison Based on Halogen Bond. *Chem. Rev.* **2016**, *116*, 5072–5104. [CrossRef] [PubMed]
18. Echeverría, J. Intermolecular Carbonyl···Carbonyl Interactions in Transition-Metal Complexes. *Inorg. Chem.* **2018**, *57*, 5429–5437. [CrossRef]
19. Doppert, M.T.; van Overeem, H.; Mooibroek, T.J. Intermolecular π-hole/n→π* interactions with carbon monoxide ligands in crystal structures. *Chem. Comm.* **2018**, *54*, 12049–12052. [CrossRef]
20. Ruigrok van der Werve, A.; van Dijk, Y.R.; Mooibroek, T.J. π-Hole/n→π* interactions with acetonitrile in crystal structures. *Chem. Commun.* **2018**, *54*, 10742–10745. [CrossRef]

21. Toikka, Y.N.; Mikherdov, A.S.; Ivanov, D.M.; Mooibroek, T.J.; Bokach, N.A.; Kukushkin, V.Y. Cyanamides as π-Hole Donor Components of Structure-Directing (Cyanamide)···Arene Noncovalent Interactions. *Cryst. Growth Des.* **2020**, *20*, 4783–4793. [CrossRef]
22. Vatsadze, S.Z.; Loginova, Y.D.; dos Passos Gomes, G.; Alabugin, I.V. Stereoelectronic Chameleons: The Donor–Acceptor Dichotomy of Functional Groups. *Chem. Eur. J.* **2017**, *23*, 3225–3245. [CrossRef]
23. Gomes, G.d.P.; Loginova, Y.; Vatsadze, S.Z.; Alabugin, I.V. Isonitriles as Stereoelectronic Chameleons: The Donor–Acceptor Dichotomy in Radical Additions. *J. Amer. Chem. Soc.* **2018**, *140*, 14272–14288. [CrossRef]
24. Kinzhalov, M.A.; Ivanov, D.M.; Melekhova, A.A.; Bokach, N.A.; Gomila, R.M.; Frontera, A.; Kukushkin, V.Y. Chameleonic metal-bound isocyanides: A π-donating CuI-center imparts nucleophilicity to the isocyanide carbon toward halogen bonding. *Inorg. Chem. Front.* **2022**, *9*, 1655–1665. [CrossRef]
25. Katkova, S.A.; Mikherdov, A.S.; Kinzhalov, M.A.; Novikov, A.S.; Zolotarev, A.A.; Boyarskiy, V.P.; Kukushkin, V.Y. (Isocyano Group π-Hole)···[d -MII] Interactions of (Isocyanide)[MII] Complexes, in which Positively Charged Metal Centers (d8-M=Pt, Pd) Act as Nucleophiles. *Chem. Eur. J.* **2019**, *25*, 8590–8598. [CrossRef]
26. Mikherdov, A.S.; Kinzhalov, M.A.; Novikov, A.S.; Boyarskiy, V.P.; Boyarskaya, I.A.; Avdontceva, M.S.; Kukushkin, V.Y. Ligation-Enhanced π-Hole···π Interactions Involving Isocyanides: Effect of π-Hole···π Noncovalent Bonding on Conformational Stabilization of Acyclic Diaminocarbene Ligands. *Inorg. Chem.* **2018**, *57*, 6722–6733. [CrossRef]
27. Mikherdov, A.S.; Katkova, S.A.; Novikov, A.S.; Efremova, M.M.; Reutskaya, E.Y.; Kinzhalov, M.A. (Isocyano group)· · · lone pair interactions involving coordinated isocyanides: Experimental, theoretical and CSD studies. *CrystEngComm* **2020**, *22*, 1154–1159. [CrossRef]
28. Schmidbaur, H.; Schier, A. Aurophilic interactions as a subject of current research: An up-date. *Chem. Soc. Rev.* **2012**, *41*, 370–412. [CrossRef] [PubMed]
29. Schmidbaur, H.; Schier, A. A briefing on aurophilicity. *Chem. Soc. Rev.* **2008**, *37*, 1931–1951. [CrossRef]
30. Tiekink, E.R.T. Supramolecular assembly of molecular gold(I) compounds: An evaluation of the competition and complementarity between aurophilic (Au· · · Au) and conventional hydrogen bonding interactions. *Coord. Chem. Rev.* **2014**, *275*, 130–153. [CrossRef]
31. Mirzadeh, N.; Privér, S.H.; Blake, A.J.; Schmidbaur, H.; Bhargava, S.K. Innovative Molecular Design Strategies in Materials Science Following the Aurophilicity Concept. *Chem. Rev.* **2020**, *120*, 7551–7591. [CrossRef]
32. Weber, D.; Gagné, M.R. Aurophilicity in Gold(I) Catalysis: For Better or Worse? In *Homogeneous Gold Catalysis*; Slaughter, L.M., Ed.; Springer International Publishing: Cham, Switherland, 2015; pp. 167–211.
33. Min, H.; Xiao, G.; Liu, W.; Liang, Y. Copper-catalyzed synthesis of 2-aminobenzothiazoles from 2-iodophenyl isocyanides, potassium sulfide and amines. *Org. Biomol. Chem.* **2016**, *14*, 11088–11091. [CrossRef] [PubMed]
34. Uson, R.; Laguna, A.; Laguna, M.; Briggs, D.A.; Murray, H.H.; Fackler, J.P., Jr. (Tetrahydrothiophene)Gold(I) or Gold(III) Complexes. *Inorg. Synth.* **1989**, *26*, 85–91.
35. Sheldrick, G. SHELXT - Integrated space-group and crystal-structure determination. *Acta Cryst. Sect. A* **2015**, *71*, 3–8. [CrossRef]
36. Sheldrick, G.M. *SADABS-2008/1-Bruker AXS Area Detector Scaling and Absorption Correction*; Bruker AXS: Madison, WI, USA, 2008.
37. Dolomanov, O.V.; Bourhis, L.J.; Gildea, R.J.; Howard, J.A.; Puschmann, H. OLEX2: A complete structure solution, refinement and analysis program. *J. Appl. Crystallogr.* **2009**, *42*, 339–341. [CrossRef]
38. Ahlrichs, R.; Bär, M.; Häser, M.; Horn, H.; Kölmel, C. Electronic structure calculations on workstation computers: The program system turbomole. *Chem. Phys. Lett.* **1989**, *162*, 165–169. [CrossRef]
39. Adamo, C.; Barone, V. Toward reliable density functional methods without adjustable parameters: The PBE0 model. *J. Chem. Phys.* **1999**, *110*, 6158–6170. [CrossRef]
40. Grimme, S.; Antony, J.; Ehrlich, S.; Krieg, H. A consistent and accurate ab initio parametrization of density functional dispersion correction (DFT-D) for the 94 elements H-Pu. *J. Chem. Phys.* **2010**, *132*, 154104. [CrossRef] [PubMed]
41. Weigend, F.; Ahlrichs, R. Balanced basis sets of split valence, triple zeta valence and quadruple zeta valence quality for H to Rn: Design and assessment of accuracy. *Phys. Chem. Chem. Phys.* **2005**, *7*, 3297–3305. [CrossRef]
42. Weigend, F. Accurate Coulomb-fitting basis sets for H to Rn. *Phys. Chem. Chem. Phys.* **2006**, *8*, 1057–1065. [CrossRef]
43. Bader, R.F.W. A quantum theory of molecular structure and its applications. *Chem. Rev.* **1991**, *91*, 893–928. [CrossRef]
44. Contreras-García, J.; Johnson, E.R.; Keinan, S.; Chaudret, R.; Piquemal, J.-P.; Beratan, D.N.; Yang, W. NCIPLOT: A Program for Plotting Noncovalent Interaction Regions. *J. Chem. Theor. Comput.* **2011**, *7*, 625–632. [CrossRef]
45. Humphrey, W.; Dalke, A.; Schulten, K. VMD: Visual molecular dynamics. *J. Mol. Graph.* **1996**, *14*, 33–38. [CrossRef]
46. Becke, A.D.; Edgecombe, K.E. A simple measure of electron localization in atomic and molecular systems. *J. Chem. Phys.* **1990**, *92*, 5397–5403. [CrossRef]
47. Lu, T.; Chen, F. Multiwfn: A multifunctional wavefunction analyzer. *J. Comput. Chem.* **2012**, *33*, 580–592. [CrossRef]
48. Yamada, S.; Rokusha, Y.; Kawano, R.; Fujisawa, K.; Tsutsumi, O. Mesogenic gold complexes showing aggregation-induced enhancement of phosphorescence in both crystalline and liquid-crystalline phases. *Faraday Discuss.* **2017**, *196*, 269–283. [CrossRef]
49. Ruch, A.A.; Ellison, M.C.; Nguyen, J.K.; Kong, F.; Handa, S.; Nesterov, V.N.; Slaughter, L.M. Highly Sterically Encumbered Gold Acyclic Diaminocarbene Complexes: Overriding Electronic Control in Regiodivergent Gold Catalysis. *Organometallics* **2021**, *40*, 1416–1433. [CrossRef]
50. Ecken, H.; Olmstead, M.M.; Noll, B.C.; Attar, S.; Schlyer, B.; Balch, A.L. Effects of anions on the solid state structures of linear gold(I) complexes of the type (o-xylyl isocyanide)gold(I) (monoanion). *J. Chem. Soc. Dalton Trans.* **1998**, 3715–3720. [CrossRef]

51. Fujisawa, K.; Okuda, Y.; Izumi, Y.; Nagamatsu, A.; Rokusha, Y.; Sadaike, Y.; Tsutsumi, O. Reversible thermal-mode control of luminescence from liquid-crystalline gold(I) complexes. *J. Mater. Chem. C* **2014**, *2*, 3549–3555. [CrossRef]
52. Bondi, A. van der Waals Volumes and Radii. *J. Phys. Chem.* **1964**, *68*, 441–451. [CrossRef]
53. Bondi, A. van der Waals Volumes and Radii of Metals in Covalent Compounds. *J. Phys. Chem.* **1966**, *70*, 3006–3007. [CrossRef]
54. Alvarez, S. A cartography of the van der Waals territories. *Dalton Trans.* **2013**, *42*, 8617–8636. [CrossRef]
55. Hashmi, A.S.K.; Hengst, T.; Lothschütz, C.; Rominger, F. New and Easily Accessible Nitrogen Acyclic Gold(I) Carbenes: Structure and Application in the Gold-Catalyzed Phenol Synthesis as well as the Hydration of Alkynes. *Adv. Synth. Catal.* **2010**, *352*, 1315–1337. [CrossRef]
56. Hobbollahi, E.; List, M.; Redhammer, G.; Zabel, M.; Monkowius, U. Structural and photophysical characterization of gold(I) complexes bearing naphthyl chromophores. *Inorg. Chem. Commun.* **2016**, *65*, 24–27. [CrossRef]
57. Katkova, S.A.; Mikherdov, A.S.; Sokolova, E.V.; Novikov, A.S.; Starova, G.L.; Kinzhalov, M.A. Intermolecular (Isocyano group)···PtII interactions involving coordinated isocyanides in cyclometalated PtII complexes. *J. Mol. Struct.* **2022**, *1253*, 132230. [CrossRef]
58. Mikherdov, A.S.; Jin, M.; Ito, H. Exploring Au(i) involving halogen bonding with N-heterocyclic carbene Au(i) aryl complexes in crystalline media. *Chem. Sci.* **2023**, *14*, 4485–4494. [CrossRef] [PubMed]
59. Aliyarova, I.S.; Tupikina, E.Y.; Ivanov, D.M.; Kukushkin, V.Y. Metal-Involving Halogen Bonding Including Gold(I) as a Nucleophilic Partner. The Case of Isomorphic Dichloroaurate(I)·Halomethane Cocrystals. *Inorg. Chem.* **2022**, *61*, 2558–2567. [CrossRef] [PubMed]
60. Aliyarova, I.S.; Tupikina, E.Y.; Soldatova, N.S.; Ivanov, D.M.; Postnikov, P.S.; Yusubov, M.; Kukushkin, V.Y. Halogen Bonding Involving Gold Nucleophiles in Different Oxidation States. *Inorg. Chem.* **2022**, *61*, 15398–15407. [CrossRef] [PubMed]
61. Desiraju, G.R.; Ho, P.S.; Kloo, L.; Legon, A.C.; Marquardt, R.; Metrangolo, P.; Politzer, P.; Resnati, G.; Rissanen, K. Definition of the halogen bond (IUPAC Recommendations 2013). *Pure Appl. Chem.* **2013**, *85*, 1711–1713. [CrossRef]
62. Ibrahim, M.A.A.; Saeed, R.R.A.; Shehata, M.N.I.; Ahmed, M.N.; Shawky, A.M.; Khowdiary, M.M.; Elkaeed, E.B.; Soliman, M.E.S.; Moussa, N.A.M. Type I-IV Halogen· · · Halogen Interactions: A Comparative Theoretical Study in Halobenzene· · · Halobenzene Homodimers. *Int. J. Mol. Sci.* **2022**, *23*, 3114. [CrossRef]
63. Selvakumar, K.; Singh, H.B. Adaptive responses of sterically confined intramolecular chalcogen bonds. *Chem. Sci.* **2018**, *9*, 7027–7042. [CrossRef]

Disclaimer/Publisher's Note: The statements, opinions and data contained in all publications are solely those of the individual author(s) and contributor(s) and not of MDPI and/or the editor(s). MDPI and/or the editor(s) disclaim responsibility for any injury to people or property resulting from any ideas, methods, instructions or products referred to in the content.